

Operator-Independent Isotropic Three-Dimensional Magnetic Resonance Imaging for Morphology in Congenital Heart Disease A Validation Study

Thomas Sangild Sørensen, MSc; Hermann Körperich, PhD; Gerald F. Greil, MD;
Joachim Eichhorn, MD; Peter Barth, MSc; Hans Meyer, MD;
Erik Morre Pedersen, MD, PhD; Philipp Beerbaum, MD

Background—Operator-independent isotropic 3D MRI may greatly simplify the assessment of complex morphology in congenital heart disease. We sought to evaluate the reliability of this new approach.

Methods and Results—In 31 adolescent and adult patients (age, 6 to 42 years; median, 16 years) with congenital heart disease, cardiac morphology was determined with free-breathing (navigator-gated), isotropic, 3D steady-state free-precession (3D SSFP) MRI and independently evaluated by 2 observers. Cardiac diagnoses and multiple distance measurements were compared with conventional MR reference sequences (ie, spin-echo, cine gradient-echo, contrast-enhanced MR angiography) and with echocardiography/cine cardioangiography or surgery. Of the 31 patients, 24 had native congenital heart defects or residual defects after repair that warranted immediate treatment. None of these defects was missed by 3D SSFP. Novel diagnostic issues were discovered in 4 of 31 patients (coronary anomalies, n=3; left juxtaposition of the right atrial appendage in double-outlet right ventricle and transposition of the great arteries, 1). For sizes of valves and vessels, we found minor mean differences of -1.1 to 1.6 mm, with SD ranging from 1.2 to 2.9 mm, demonstrating overall good agreement with standard MRI (Bland-Altman analysis). Interobserver variability of 3D SSFP distance measures was low; mean differences ranged from -1.5 to 1.0 mm, and SD ranged from 0.8 to 2.5 mm. Scatter was lower for extracardiac than intracardiac measures.

Conclusions—In adolescents and adults, isotropic 3D SSFP MRI allows reliable assessment of complex cardiac morphology. Distance measurements are accurate and reproducible. Thus, a single operator-independent acquisition may substitute for conventional 2D MRI sequences to accelerate and simplify MR scanning in congenital heart disease. (*Circulation*. 2004;110:163-169.)

Key Words: computers ■ heart defects, congenital ■ magnetic resonance imaging ■ pediatrics

Cardiac MRI has become a clinically useful addition to echocardiography in the diagnosis and follow-up of patients with congenital heart disease (CHD). Such 2D MRI sequences as multislice spin-echo and cine gradient-echo angiography have been validated in the diagnosis of chamber morphology,¹ complex heterotaxy syndromes,² ventricular (VSDs) and atrial (ASDs) septal defects,^{3,4} valvular diseases,⁵ and different types of pathology of the great thoracic vessels.⁶ Diagnostic cardiac catheterization can thus be frequently avoided.¹

The widespread use of MRI in CHD, however, is hampered by the complex nature of the multiple 2D MR scanning

protocols and the need for highly individualized planning procedures.⁷ Recently, 3D contrast-enhanced MR angiography (MRA) has been shown to be an important improvement in the field. The 3D nature of these data allows reformatting in any desired image plane during postprocessing,^{8,9} which constitutes a first step in obtaining MR data in a less operator-dependent manner. Because of the usually ECG-untriggered acquisition, however, contrast-enhanced MRA is intended primarily for extracardiac rather than intracardiac morphology.^{8,9} Moreover, because data are often acquired nonisotropically, optimal image resolution is available in only 1 projection.

Received January 6, 2004; revision received March 16, 2004; accepted March 23, 2004.

From the Department of Cardiothoracic Surgery (T.S.S.) and MR Center (T.S.S., E.M.P.), Institute of Experimental Clinical Research, Skejby Hospital, Aarhus University Hospital, Aarhus, Denmark; Clinic for Congenital Heart Disease and Institute for Magnetic Resonance Imaging, Heart and Diabetescenter Northrhine Westfalia, Ruhr University of Bochum, Bochum, Germany (H.K., P.B., H.M., P.B.); University Hospital of Tübingen, Department of Pediatric Cardiology, Tübingen, Germany (G.F.G.); and University Hospital of Heidelberg, Department of Pediatric Cardiology, Heidelberg, Germany (J.E.).

Movies are available in the online-only Data Supplement at <http://www.circulationaha.org>.

Correspondence to Philipp Beerbaum, MD, Clinic for Congenital Heart Disease, Heart and Diabetes Center Northrhine-Westfalia, Ruhr University of Bochum, Georgstr 11, D-32545 Bad Oeynhausen, Germany. E-mail pbeerbaum@hdz-nrw.de

© 2004 American Heart Association, Inc.

Circulation is available at <http://www.circulationaha.org>

DOI: 10.1161/01.CIR.0000134282.35183.AD

With the advent of steady-state free-precession (SSFP) MRI, 3D acquisitions can now be obtained isotropically, flow independently, and time-efficiently without contrast injections.^{10,11} A 3D SSFP sequence can image both intracardiac and extracardiac morphology when triggered to a small window in the cardiac cycle. Instead of a series of 2D nonisotropic slices being acquired, possibly with different angulations, all information can be contained in a single, operator-independent acquisition. The isotropic property of the data allows arbitrary reformatting of any desired imaging plane without loss of resolution. Thus, the morphological evaluation may be performed during postprocessing, for which dedicated evaluation software has recently been introduced.¹² Compared with conventional imaging, this constitutes a greatly simplified procedure. We designed a study to prospectively evaluate the clinical utility and diagnostic accuracy of isotropic 3D SSFP MRI for morphology in CHD. We defined 4 study hypotheses. First, there is a lower limit in age and body size at which isotropic 3D SSFP is feasible. Second, isotropic 3D SSFP can be acquired operator independently and used to assess both intracardiac and extracardiac anatomy in a simplified and standardized manner. Complete diagnoses of congenital heart malformations or residual defects can be made offline by interactive planar reformatting by different observers. Third, quantitative distance measurements in the 3D SSFP data can be obtained with low interobserver variability. And fourth, there is good agreement in quantitative distance measurements between dedicated reformatted image planes of the isotropic 3D SSFP data sets and the analogous conventional 2D slices or 3D contrast-enhanced MRA projections.

Methods

Study Population

From April to October 2003, we prospectively enrolled into the study 56 patients (age, 0 to 42 years; median, 10 years) with a variety of both preoperative and postoperative congenital heart defects. All patients were clinically referred for further diagnostic evaluation by MRI because either a significant residual defect was suspected or transthoracic echocardiography was unable to visualize the relevant cardiovascular morphology. All patients were in sinus rhythm. Informed, written consent was obtained from the patient, parents, or caretakers.

Study Design

Each patient received an isotropic 3D SSFP scan triggered to end diastole, followed by the conventional MRI examination, including multislice spin-echo, cine gradient-echo, and 3D contrast-enhanced angiography.³

First, to evaluate hypothesis 1, all 52 of the 3D SSFP data sets were initially graded according to Table 1 (T.S.S., P. Beerbaum) to determine the relation of age, body size, and image quality. Data sets with a grade of <3 were excluded from further evaluation (n=21), and a comparison between the characteristics of these patients and those with data quality of grade of >3 was made (see Results).

Second, we invited 2 experienced independent observers (G.F.G., J.E.) to evaluate solely the 31 selected 3D SSFP data by making complete structural diagnoses, including segmental morphology and residual defects (hypothesis 2); performing distance measurements at predefined anatomical sites for definition of interobserver variation (hypothesis 3); and semiquantitatively assessing image quality according to Table 1.

TABLE 1. Scoring System⁸

Score	Description
1	Poor-quality information: nondiagnostic
2	Structures visible but markedly blurred: diagnosis suspected but not established
3	Anatomy visible with moderate blurring: able to establish diagnosis
4	Minimal blurring: good-quality diagnostic information with definite diagnosis
5	Sharply defined borders: excellent-quality diagnostic information

Both observers were blinded to each other's results. In preoperative cases with no previous surgery or only palliative surgery, no patient-specific information was passed to the observers. In postoperative cases, the surgical history was provided, but we asked for the diagnosis of any residual problem. The observers were unaware of whether such a residual defect was present in a certain case. The 3D SSFP-based diagnoses were compared with reference diagnostics obtained from the conventional MRI, echocardiography, and if available, from cardiac catheterization or surgery.

Third, to evaluate hypothesis 4 and to provide a quantitative comparison of 3D SSFP and conventional MRI, we acquired both intracardiac and extracardiac measures separately and blinded. One set of reference measures was obtained in the conventionally obtained MRI images (E.M.P.), all acquired in end diastole or otherwise left out. These measures were then compared separately with both sets of 3D SSFP observer measurements (observer 1, G.F.G.; observer 2, J.E.).

Measurement Sites

Transversal Planes

Transversal planes included the inferior vena cava just below the entrance to the right atrium (measurements left to right), superior vena cava (SVC) at the level of the right pulmonary artery (measurements left to right), minimum diameters of right and left pulmonary arteries halfway between the offspring and lobe branches, and ascending aorta at the level of the pulmonary bifurcation (measurements left to right).

Sagittal Planes

Sagittal planes were the aortic arch (between the left common carotid and left subclavian artery), aortic isthmus, descending aorta (level of diaphragm), and main pulmonary artery at the level of the pulmonary valve.

Four-Chamber View

Using the 4-chamber reference acquisitions, we automatically reformatted identical slices in the 3D SSFP acquisition to avoid measurement errors resulting from angulation differences for the width of the tricuspid and mitral valve orifices.

MRI Technique

All examinations were performed on a 1.5-T whole-body MR scanner (ACS-NT, Philips Medical Systems; maximum gradient performance, 30 mT/m amplitude; slew rate, 150 T · m⁻¹ · s⁻¹) with a 5-element cardiac coil. Detailed descriptions of conventional MRI sequence settings have been given elsewhere.³ For contrast-enhanced MRA (final scan), gadolinium DTPA (Magnevist) was applied at a dose of 0.2 mmol/kg with an injection rate of 2.0 to 3.0 mL/s or by hand injection as appropriate.

Table 2 summarizes the settings of the isotropic 3D SSFP sequence for the patients included for diagnostic evaluation (see Results). The 3D volumes were obtained in a standardized, operator-independent manner covering the cardiovascular structures sagittally between the level of the diaphragm and the neck. Scanning was performed during free breathing with a navigator on the right hemidiaphragm for prospective motion correction. A spectrally

TABLE 2. Isotropic 3D-SSFP Protocol of the 31 Patients Included for Diagnostic Evaluation

Property	Young Children (n=6; age, 6–8 y)	Adolescents and Adults (n=25; age, 9–42 y)
Field of view, mm	140–160	330
Matrix (voxels)	80–96×80–96	160×160
Rectangular field of view, %	100	65–100
Isotropic resolution, mm ³	1.5–1.8	2.1
Slices, n	70–100	60–120
k-Space segmentation factor	13	20–26
Averages, n	2	1
Acquisition window, ms	45–55	80–100
Total scan duration, including navigator (mean), min	6:44	3:42
Navigator window, mm	No navigator (n=2) 3 (n=4)	3–5 (n=15) 6–7 (n=10)
Mean heart rate (range), bpm	88/70–100	75/58–94
SENSE factor	No SENSE (n=3) 1.3–1.5 (n=3)	No SENSE (n=21) 1.3–1.8 (n=4)
T ₂ preparation pulse, ms	25	35
Repetition time (mean±SD), ms	4.0±0.3	3.6±0.1
Echo time (mean±SD), ms	2.0±0.1	1.8±0.1

SENSE indicates sensitivity encoding.¹⁸

All 3D-SSFP acquisitions: sagittal image plane orientation; 90° flip angle; selective fat saturation prepulse; maximum trigger delay (end diastole); and free breathing.

selective fat saturation pulse and a T₂ prepulse¹³ were used to increase the contrast between blood, fat, and myocardium.

MRI Analysis

Dedicated software was used for interactive planar reformatting of arbitrary imaging planes of the isotropic volume. Observers were able to explore the imaging volume in real time by interactively defining the desired imaging angulation and offset. Local maximum-intensity projections could be used in any imaging plane (Figures 1 and 2). Furthermore, this article has an accompanying movie available online (see the Data Supplement available at <http://www.circulationaha.org>) that provides an example of an interactive diagnostic session in a patient with d-transposition of the great arteries (d-TGA) and Mustard repair.

Statistical Analysis

The analysis of Bland and Altman¹⁴ was used to evaluate the agreement of measures between conventional reference scans and 3D SSFP scans and to determine interobserver variability of measures in the 3D SSFP data sets.

Results

The 3D SSFP scans were completed successfully in 52 of the 56 patients. Two patients failed to cope with the navigator, and suboptimal initial shimming caused severe signal void in another 2 patients. In another 3 patients, data were reacquired after a new shimming volume was defined as a result of signal void in parts of the volume.

Age Limitation Based on Image Quality Scoring (Hypothesis 1)

In 21 patients (age, 0 to 7 years; median age, 3 years; mean heart rate, 115 bpm; range, 86 to 145 bpm), image quality was graded 1 or 2 with a mean score of 1.9, whereas in 31 patients (age, 6 to 42 years; median, 16 years), the quality was rated ≥ 3 . Age of >7 years, weight of >20 kg, and heart rate <100 bpm constituted the borderline with only 1 exception, a 6-year-old girl with aortic coarctation. Thus, a clear distinction in image quality separated infants and younger children (n=21) from adolescents and adults (n=31).

In the group of 31 patients included in further analysis by an initial 3D SSFP image quality score ≥ 3 (Table 1), image quality was reassessed independently by the 2 observers with average scores of 4.3 and 4.5. The average scan duration was 4:20 minutes (range, 2:38 to 10:30 minutes). Eighty percent (25 of 31) were completed in <5 minutes. Navigator efficiency was typically $\approx 50\%$. The average heart rate was 78 bpm (range, 58 to 100 bpm). Sedation was necessary in 5 children unable to cooperate.

Segmental Cardiac Morphology by 3D SSFP (Hypothesis 2)

The morphological analysis could take from a few minutes to lay out a simple coarctation to 20 to 30 minutes for the full segmental description and diagnosis in the complex cases.

Although there was a high rate of complex and significant CHD, no mistakes of clinical relevance were made by any observer in assessing segmental cardiac morphology, situs, native defects, and residual lesions by 3D SSFP. In 29 of 31 cases, both observers established a 100% identical and correct morphological diagnosis (compared with all references) based entirely on 3D SSFP. Both missed a thickened aortic valve in 1 case, and a reported ASD (8-year-old boy) by 1 observer was not confirmed by echocardiography.

A summary of all patient diagnoses by reference methods (correctly described by 3D SSFP) follows.

1. d-TGA and Mustard atrial baffle: n=5; age range, 12 to 25 years. Severe SVC obstruction (n=2), SVC occlusion (n=1; Figure 1). All had previous cardiac catheterization but too long ago to describe the residual defect.
2. Tetralogy of Fallot postrepair: n=5; age range, 8 to 42 years. Relevant pulmonary regurgitation and branch pulmonary artery stenosis (n=4). Valvular homograft stenosis (n=1). Right-side heart dilatation, branch stenoses, and presence of right aortic arch (n=3) confirmed by cardiac catheterizations in 4 patients (balloon dilatation of branch pulmonary stenosis).
3. ASDs: Sinus-venous ASDs, n=2; age, 15 and 18 years, with partial anomalous pulmonary venous return from the right lung (Figure 2a), right-side heart dilatation, and a persisting left SVC draining to the coronary sinus (n=2). Confirmation at surgery. One residual inferior ASD (Figure 2b) confirmed at cardiac catheterization.
4. VSD: n=3; age, 6 to 16 years. Two native perimembranous and 1 residual muscular postrepair. Reference by echocardiography.

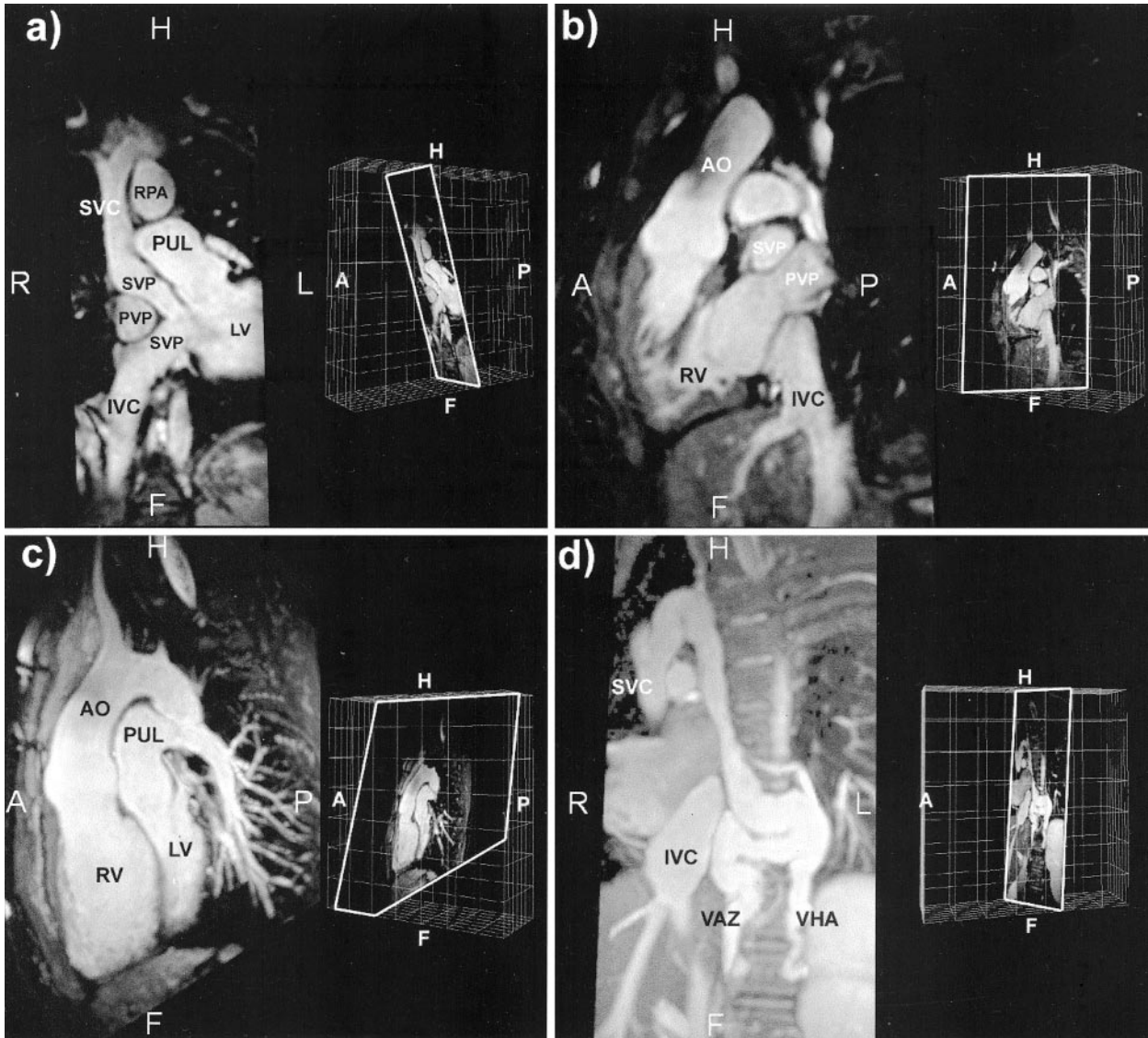


Figure 1. Four reformatted planes from isotropic 3D SSFP acquisitions in 2 patients with d-TGA and Mustard atrial switch. In each quadrant, wire-frame box represents acquired volume in which white frame marks chosen reformatted slice as shown on left. A, B, Unobstructed systemic venous pathways (SVP; A) from inferior vena cava (IVC) and SVC to left ventricle (LV), as well as pulmonary venous pathway (PVP; B) toward right ventricle (RV). C, d-TGA, aorta (AO), pulmonary artery (PUL), 13-mm maximum intensity projection, left lateral view. D, Obstructed upper systemic venous pathway in another patient with d-TGA and Mustard repair. Note enlarged vena azygos (VAZ) and vena hemiazygos (VHA) leading blood from SVC to IVC, thus bypassing obstruction; 8-mm maximum intensity projection. A indicates anterior; P, posterior; f, feet; H, head; R, right; L, left; LA, left atrium; LV, left ventricle; RA, right atrium; and RPA, right pulmonary artery.

5. Pulmonary atresia with VSD, n=2; age, 18 years for both; 1 with Waterston-Cooley-Shunt. Correct delineation of anatomy and any major aortopulmonary collateral arteries included in the 3D SSFP volume. Moreover, hypoplastic central pulmonary arteries and their connections with major aorto-pulmonary collateral arteries correctly diagnosed by both observers. Previous cardiac catheterizations available.
6. Coarctation of the aorta: native (n=4; age, 6 to 8 years; recent catheterization available) and postsurgical (n=3; age, 11 to 17 years). Kinking (Figure 2c) of the arch in 2 patients. Relevant collaterals visualized by 3D SSFP if included in the volume.
7. Miscellaneous (n=6; no recent catheterizations). Complete concordance of 3D SSFP with reference MR. Sup-

ravalvular main pulmonary artery stenosis after debanding of the pulmonary artery and VSD closure (n=1; age, 36 years). Supravalvular stenosis of ascending aorta; displaced origins of both coronary arteries visualized only by 3D SSFP (n=1; age, 16 years). d-TGA with VSD, pulmonary valve stenosis, and aorto-pulmonary collaterals (n=1; age, 41 years; Figure 2d). Double-outlet right ventricle with l-TGA, VSD, pulmonary valve stenosis, postrepair (n=1; age, 15 years); relevant pulmonary homograft incompetence. Tricuspid atresia with l-TGA (n=1; age, 9 years) after Glenn shunt and pulmonary banding; loose PA band; left-sided pulmonary hypertension. Pulmonary atresia/intact ventricular septum (n=1; age, 12 years) after valve commissurotomy and Waterston shunt; right pulmonary branch stenosis.

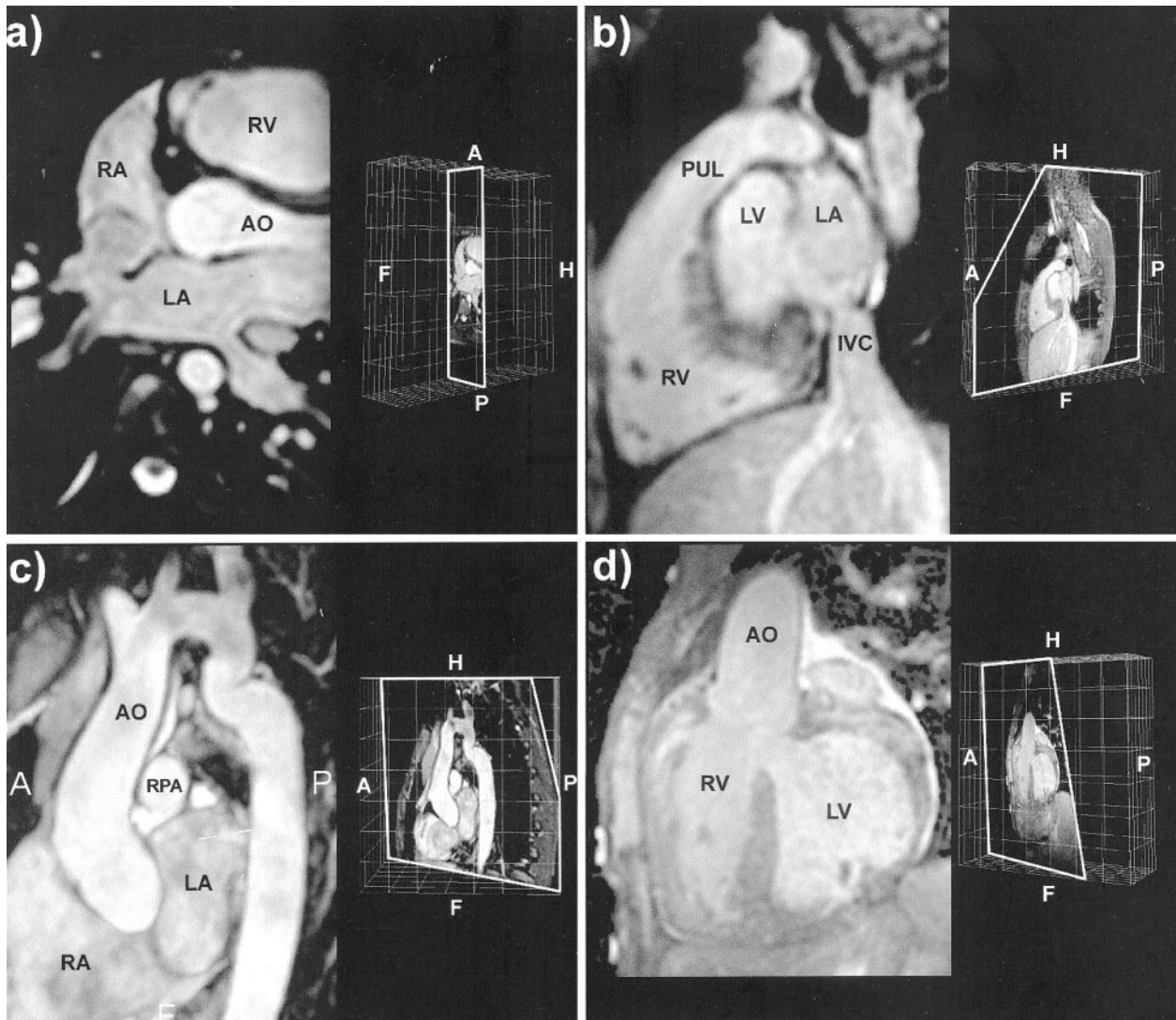


Figure 2. Reformatted isotropic 3D SSFP in 4 clinical examples. In each quadrant, wire-frame box represents acquired volume in which white frame marks chosen reformatted slice as shown on left. A, Sinus-venous ASD with anomalous return of right upper pulmonary vein. B, Residual ASD allows right-to-left shunting of blood from inferior vena cava (IVC) to left atrium (LA). C, Kinking aortic arch, 5-mm maximum intensity projection. D, d-TGA, VSD, and severe pulmonary stenosis. Septal defect and aortic outflow tract (AO) are visible in selected slice. Abbreviations as in Figure 1.

Overall, only 4 patients had no postrepair residual defects (ie, 3 postcoarctation, 1 Mustard/d-TGA), and 3 had insignificant native CHD (2 small VSD, 1 kinking of aortic arch). Thus, only 7 of 31 (23%) did not need any therapy, whereas 24 of 31 (77%) needed either surgery or cardiac intervention. Moreover, in 4 patients, novel information was available only in 3D SSFP data (origin, size, proximal course and patency of coronary arteries ($n=3$); identification of left juxtaposition of the right atrial appendage in the patient with double-outlet right ventricle and transposed arteries).

Quantitative Measures in 3D SSFP

Interobserver comparison (Bland-Altman analysis) of measures from the 3D SSFP acquisition by the 2 blinded observers (hypothesis 3; Table 3) revealed negligible mean differences (-1.5 to 1.0 mm) with SD ranging from 0.8 to 2.5 mm. Hence, the means and limits of agreement showed

compatible measures from all extracardiac anatomy and from the AV valves.

Table 4 summarizes the results of the Bland-Altman analysis comparing the blinded intracardiac and extracardiac 3D SSFP measures with the obtained reference measurements (hypothesis 4). We observed overall close agreement, with extracardiac measures showing less variance than intracardiac measures.

Discussion

A New Scanning Strategy

Although of increasing importance, MR scanning to assess morphology in CHD is currently a demanding and difficult technique. Usually, a series of multiple spin-echo and gradient-echo 2D slices is obtained anisotropically for intracardiac morphology and function, followed by 3D contrast-enhanced MRA for extracardiac morphology. Considerable

TABLE 3. Calculation of Interobserver Variance of Intracardiac and Extracardiac Measurements in 3D-SSFP With Bland-Altman Analysis¹⁴

Measurement Site	Mean Difference, mm	Lower/Upper Limits of Agreement,* mm
Inferior vena cava	0.1	-3.0/3.1
Superior vena cava	-0.7	-3.0/1.6
Main pulmonary artery	0.4	-3.0/3.7
Right pulmonary artery	-0.5	-2.0/1.0
Left pulmonary artery	-0.8	-3.5/1.8
Aorta, ascending	-1.0	-3.3/1.3
Aorta, arch	-0.9	-3.3/1.5
Aorta, isthmus	-1.5	-4.1/1.0
Aorta, descending	-0.8	-2.8/1.2
Tricuspid valve	1.0	-3.0/5.0
Mitral valve	0.4	-4.6/5.4

*Mean \pm 2 SD.

planning efforts are often needed to position and obtain the desired imaging planes and multiple acquisitions, with breathholding adding to the complexity. Hence, a thorough MR investigation is time-consuming and requires a highly skilled and dedicated investigator.

Theoretically, 2 alternative approaches may circumvent this challenge. First, real-time imaging¹⁵ may be used to interactively angulate and position exactly the desired imaging planes. Although appealing, current implementations lack the necessary image resolution. Furthermore, real-time MRI would still be user dependent, and additional imaging planes could not be acquired once a session was finished.

The second possible approach is introduced in this article: With a free-breathing, isotropic, 3D acquisition to cover the entire heart,¹⁰ any imaging plane can be consequently reformatted in real time by interactive postprocessing. Because the planning process involves only the definition of a box around the heart, it is considered to be operator independent. As

proved by our 2 independent observers, the morphological diagnosis can be determined any time after the acquisition, and the cardiologist/radiologist can be freed from the task of performing the actual acquisition.

This approach should be accompanied, however, by a number of cine sequences³ and flow acquisitions.¹⁶ Currently, such functional studies are obtained as anisotropic single-slice or multislice acquisitions. Advances toward isotropic 3D imaging for these sequences also would eventually provide benefits comparable to those that we have demonstrated for the morphological single-phase 3D SSFP scan. Emerging acceleration techniques¹⁷ will be important in reaching this goal.

3D SSFP: Diagnostic Results

Although the prevalence of significant CHD was high in our population, none of these defects/residua were missed or ill defined by the observers looking solely at the 3D SSFP data compared with reference MRI, echocardiography, cardiac catheterization, or surgery. Moreover, coronary anomalies and unsuspected diagnoses such as left juxtaposition of right atrial appendage were visualized only in the 3D SSFP data. The basis for this was an overall good image quality, with an average grading of 4.4 (Table 1). The good performance of both observers is remarkable because clinical background information was kept sparse to avoid bias from any diagnostic clue. Hence, we proved hypothesis 2, which states that a single isotropic 3D SSFP MRI may successfully be substituted for a range of conventional acquisitions to delineate complex morphology.

3D SSFP: Quantitative Validation

The multiple intracardiac and extracardiac distance measurements obtained in the 3D SSFP data showed compatible measures between both observers (Table 3). This is an indication of good image contrasts (sharp borders) as confirmed by the blinded observer grading. The scatter was slightly higher for intracardiac than extracardiac measures. This finding can be explained by less reproducibility of the exact

TABLE 4. Comparison of Intracardiac and Extracardiac Measures Between 3D-SSFP (Observers) and Conventional 2D Imaging (Reference) With Bland-Altman Analysis¹⁴

Measurement Site	Observer 1		Observer 2	
	Mean Difference, mm	Lower/Upper Limits of Agreement,* mm	Mean Difference, (mm)	Lower/Upper Limits of Agreement,* mm
Inferior vena cava	-0.1	-3.7/3.5	0.1	-3.4/3.7
Superior vena cava	-0.6	-3.2/2.0	-0.1	-2.5/2.3
Main pulmonary artery	-0.3	-3.5/2.9	-0.7	-3.4/2.0
Right pulmonary artery	-0.3	-3.0/2.3	0.1	-2.5/2.7
Left pulmonary artery	-0.7	-3.7/2.3	0.0	-2.4/2.3
Aorta, ascending	-1.1	-3.9/1.7	-0.2	-3.7/3.4
Aorta, arch	-0.8	-3.9/2.2	0.1	-2.7/3.0
Aorta, isthmus	-1.0	-3.5/1.4	0.7	-2.0/3.3
Aorta, descending	-0.6	-3.3/2.1	0.2	-2.6/2.9
Tricuspid valve	0.5	-5.2/6.2	1.6	-4.0/7.2
Mitral valve	0.2	-5.4/5.8	0.9	-4.7/6.4

*Mean \pm 2 SD.

measurement sites of valve measurements compared with vessel measurements because the valve leaflets were not visible in all data sets. Also, for the comparative measures between the breathhold 2D cine SSFP reference scans and the navigator-guided 3D SSFP scans, it was not possible to fully compensate for variations in the diaphragm position, causing measurements in slightly different 4-chamber imaging planes. On the basis of the overall observer agreement, however, we proved hypothesis 3, stating that morphological measurements are reliable even when different observers are involved.

Additionally, when measures from 3D SSFP are compared with reference measures from conventional acquisitions (Table 4), the Bland-Altman analyses showed good agreement. On the basis of this quantitative validation, we proved hypothesis 4, namely that a single operator-independent acquisition can assess distance measurements accurately and thus depict both intracardiac and extracardiac anatomy in a simplified and standardized manner.

3D SSFP: Age Limitation

On the basis of the initial grading of all imaging data, the youngest age at which isotropic 3D SSFP imaging is applicable was determined to be ≈ 7 years, thus proving our hypothesis 1. Although we did increase isotropic resolution to 1.6 mm³ in younger patients, we observed blurring and low signal- and contrast-to-noise ratios.

In the 6 younger patients (6 to 8 years of age) who were included with good image quality, we used a considerably shorter acquisition duration (45 to 55 ms) compared with the older subjects (80 to 100 ms; see Table 2). Interestingly, the heart rate in this group was only a little higher than in the older group (younger subjects: mean, 88 bpm; range, 77 to 100 bpm; older subjects: mean, 75 bpm; range, 58 to 94; Table 2). In contrast, in the excluded 21 patients, the mean heart rate was clearly higher (mean, 115 bpm; range, 86 to 145). The use of sensitivity encoding,¹⁸ repetition time/echo time durations, acquisition durations, or patient compliance did not provide a consistent explanation for the reduced image quality in this group.

We assume that, among a number of contributing factors, heart rate plays the most important role. Further research should focus on the definition of the length of diastolic rest period at a higher heart rate. The acquisition duration may have to be further reduced and/or more precisely shifted to the diastolic rest period by choosing an appropriately defined trigger delay. Moreover, the different tissue relaxation behavior at different heart rates may deserve closer consideration.

Study Limitations

No conclusions from our data are applicable to patients with arrhythmia. It was not always possible to delineate the entire atrial septum and cardiac valves, even though cardiac valves were visible in >50% (with the pulmonary valve being the exception). These shortcomings of 3D SSFP, however, also apply to conventional spin-echo and single-phase gradient-echo imaging. Such gaps can usually be accommodated by Doppler echocardiography or a multiphase 2D-SSFP scan.⁵ Moreover, a supplementary MR flow acquisition may accurately size ASDs.⁴

Conclusions

The 3D SSFP is reliable, accurate, and time efficient in the assessment of morphology in CHD and may replace conven-

tional 2D scanning. The sequence can be acquired operator independently, and the diagnostic workup can be performed exclusively in postprocessing by real-time interactive planar reformatting. This is an important step toward a simplified and standardized examination of the growing number of adolescents and adults with CHD.

Acknowledgments

We thank the Danish Heart Foundation (grant 01-2-3-27A-22924), Danish Agency for Trade and Industry (through EUREKA project 2061; INCA-MRI), Danish Medical Research Council (grant 28809), the Karen Elise Jensen Foundation, ELHKE Foundation, and Philips Medical Systems, which helped fund this project.

References

- Boxt LM, Rozenshtein A. MR imaging of congenital heart disease. *Magn Reson Imaging Clin N Am*. 2003;11:27-48.
- Geva T, Vick GW 3rd, Wendt RE, et al. Role of spin echo and cine magnetic resonance imaging in presurgical planning of heterotaxy syndrome: comparison with echocardiography and catheterization. *Circulation*. 1994;90:348-356.
- Chung T. Assessment of cardiovascular anatomy in patients with congenital heart disease by magnetic resonance imaging. *Pediatr Cardiol*. 2000;21:18-26.
- Beerbaum P, Korperich H, Esdorn H, et al. Atrial septal defects in pediatric patients: noninvasive sizing with cardiovascular MR imaging. *Radiology*. 2003;228:361-369.
- Glockner JF, Johnston DL, McGee KP. Evaluation of cardiac valvular disease with MR imaging: qualitative and quantitative techniques. *Radiographics*. 2003;23:e9.
- Holmqvist C, Stahlberg F, Hanseus K, et al. Collateral flow in coarctation of the aorta with magnetic resonance velocity mapping: correlation to morphological imaging of collateral vessels. *J Magn Reson Imaging*. 2002;15:39-46.
- Fellows KE, Weinberg PM, Baffa JM, et al. Evaluation of congenital heart disease with MR imaging: current and coming attractions. *AJR Am J Roentgenol*. 1992;159:925-931.
- Greil GF, Powell AJ, Gildein HP, et al. Gadolinium-enhanced three-dimensional magnetic resonance angiography of pulmonary and systemic venous anomalies. *J Am Coll Cardiol*. 2002;39:335-341.
- Geva T, Greil GF, Marshall AC, et al. Gadolinium-enhanced 3-dimensional magnetic resonance angiography of pulmonary blood supply in patients with complex pulmonary stenosis or atresia: comparison with x-ray angiography. *Circulation*. 2002;106:473-478.
- Weber OM, Martin AJ, Higgins CB. Whole-heart steady-state free precession coronary artery magnetic resonance angiography. *Magn Reson Med*. 2003;50:1223-1228.
- Razavi RS, Hill DL, Muthurangu V, et al. Three-dimensional magnetic resonance imaging of congenital cardiac anomalies. *Cardiol Young*. 2003;13:461-465.
- Sorensen TS, Pedersen EM, Hansen OK, et al. Visualization of morphological details in congenitally malformed hearts: virtual three-dimensional reconstruction from magnetic resonance imaging. *Cardiol Young*. 2003;13:451-460.
- Brittain JH, Hu BS, Wright GA, et al. Coronary angiography with magnetization-prepared T2 contrast. *Magn Reson Med*. 1995;33:689-696.
- Bland JM, Altman DG. Statistical methods for assessing agreement between two methods of clinical measurement. *Lancet*. 1986;1:307-310.
- Guttman MA, Kellman P, Dick AJ, et al. Real-time accelerated interactive MRI with adaptive TSENSE and UNFOLD. *Magn Reson Med*. 2003;50:315-321.
- Beerbaum P, Korperich H, Gieseke J, et al. Rapid left-to-right shunt quantification in children by phase-contrast magnetic resonance imaging combined with sensitivity encoding (SENSE). *Circulation*. 2003;108:1355-1361.
- Tsao J, Boesiger P, Pruessmann KP. k-t BLAST and k-t SENSE: dynamic MRI with high frame rate exploiting spatiotemporal correlations. *Magn Reson Med*. 2003;50:1031-1042.
- Pruessmann KP, Weiger M, Scheidegger MB, et al. SENSE: sensitivity encoding for fast MRI. *Magn Reson Med*. 1999;42:952-962.